Effect of low numerical-aperture femtosecond two-photon absorption on (SU-8) resist for ultrahigh-aspect-ratio microstereolithography

W. H. Teh[a)]
IBM Research, Zürich Research Laboratory, 8803 Rueschlikon, Switzerland and Cavendish Laboratory, University of Cambridge, Madingley Road, Cambridge CB3 0HE, United Kingdom

U. Dürig and U. Drechsler
IBM Research, Zürich Research Laboratory, 8803 Rueschlikon, Switzerland

C. G. Smith
Cavendish Laboratory, University of Cambridge, Madingley Road, Cambridge CB3 0HE, United Kindom

H.-J. Güntherodt
Institute of Physics, University of Basel, Klingelbergstrasse 82, CH-4056, Basel, Switzerland

(Received 22 July 2004; accepted 14 December 2004; published online 15 February 2005)

We report the quantitative characterization and analysis on the solidification of SU-8, a chemically amplified near-ultraviolet ultrathick resist, based on two-photon-absorbed (TPA) near-infrared photopolymerization. The resolution of TPA photopolymerized SU-8 voxels and lines is studied as a function of laser-pulse energy, single-shot exposure time, and scanning speed. Two-photon microstereolithography using SU-8 as the matrix material was verified by the fabrication of SU-8 photoplastic structures with subdiffraction-limit resolution. We show that the nonlinear velocity dependence of TPA photopolymerization can be used as the shutter mechanism for disruptive three-dimensional (3D) lithography. This mechanism, when combined with low numerical-aperture optics is exploited for the rapid 3D microfabrication of ultrahigh-aspect-ratio (up to 50:1) photoplastic pillars, planes, and cage structures. © *2005 American Institute of Physics*.
[DOI: 10.1063/1.1856214]

I. INTRODUCTION

A well-controlled real three-dimensional (3D) lithography capability offers a direct route to many micromachined structures that are elements of many innovative devices with applications in micro/nanoelectromechanical systems (MEMS/NEMS), microfluidics, microphotonics, data storage, and biochemistry. Conventional lithography based on single-photon absorption (SPA) has limited spatial resolution due to diffraction and limited flexibility in direct lithographic patterning of (3D) parts due to light absorption in the resist. The former is improved by either decreasing the patterning beam wavelengths using atom, electron, or ion waves or by directly reducing the probe-specimen interaction area as done in scanning tunneling microscope (STM), atomic force microscope (AFM), and near-field scanning optical microscope (NSOM). These methods, however, abandon the use of light probe (STM, AFM) or the propagating modes of light (NSOM) and are thus, only applicable to two-dimensional (2D) imaging and fabrication.[1] One way to achieve 3D microfabrication is by piling up 2D layers but this requires accurate layer-by-layer alignment in combination with sacrificial processes. One can also exploit the nonlinearity of photopolymerization in response to beam intensity in specially prepared resins,[2] or by other innovative methods such as the "integral" process, in which a complete layer is built in a single irradiation.[3]

The two-photon-absorption (TPA) approach provides a means for photoactivating chemical and physical processes with subdiffraction-limit (SDL) spatial resolution, without the need of an external element (such as a tip) to provide local enhancement of the electromagnetic field. TPA enables 3D lithography because its excitation rate depends quadratically on light intensity. By tightly focusing a high-peak-power excitation beam into the interior of a resist with a suitable dose, the resist material can absorb two photons of light over a much smaller spatial region than would be limited by Rayleigh diffraction in conventional lithography based on SPA. The inherent nonlinear nature of TPA allows 3D lithographic production of structures since TPA is confined at the focus to a volume of the order of the cube of the excitation wavelength, without sufficient intensity to expose the nonfocused regions.[4] Several groups have utilized TPA lithography to enable the development of new technologies, such as 3D optical storage memory,[5,6] 3D fluorescence imaging of living cells,[7] 3D photonics,[8] and 2D/3D microfabrication of static[4,6,9–12] and movable[13–15] components. However, the photopolymer media used were mainly SCR-500,[1,10,11,14,16,17] or other specially prepared resin,[4–6,8,9,13] which are not widely used in the general MEMS community as compared to SU-8. This restricts rapid MEMS/NEMS prototyping work. SU-8, a negative tone, chemically amplified near-UV photoresist which was developed at IBM,[18] has most of the advantages required by the MEMS community: low-cost, low optical absorption in near UV, thermal and chemical stabilities, good resolution with vertical sidewall profiles, and ultrathick spin-on coatings. Af-

[a)]Author to whom correspondence should be addressed; electronic mail: wenghong@cantab.net

ter the introduction[19,20] of SU-8 to the MEMS community, it has found applications in masking and pattern transfer, especially in high-aspect-ratio (AR) structuring for electroplating[21] and microfluidics,[22,23] or directly used as a photoplastic material to fabricate micromechanical components, such as AFM/NSOM probes,[24–26] microgrippers,[27] microcoils,[28] and microgears.[29] It is therefore only natural for TPA lithography to be extended to SU-8 due to its familiarity, low-cost and its ultrathick spin-on coatings, the latter providing a large spatial flexibility for 3D microfabrication.

Witzgall *et al.*[12] pioneered early TPA work on SU-8, beyond which little work has been recorded, except for the recent demonstration[30] of near-field TPA on very thin layers of SU-8. The latter work, however, fails to exploit the ultrathick spin-on capabilities of SU-8. Meanwhile, Kuebler *et al.*[31] experienced limited success in their attempts to fabricate 3D structures in thick films of SU-8 containing conventional photoacid generators (i.e., triarylsulfonium cations) and have instead, resorted to synthesizing a new photoacid generator (BSB-S_2) in SU-8 in order to reliably fabricate these structures. Contrary to the experience faced by Kuebler *et al.*, we have recently demonstrated[32,33] the well-controlled two-photon microfabrication of high-fidelity 3D photoplastic structures with subdiffraction-limit resolution using only off-the-shelf ultrathick SU-8 resist (i.e., with conventional photoacid generators) as the two-photon media.

In this contribution, we report the systematic quantitative characterization and analysis of the effect of low numerical-aperture (NA) femtosecond two-photon-absorption on SU-8 for applications in ultrahigh-aspect-ratio microstereolithography. TPA near-infrared photopolymerized SU-8 voxels and lines are studied as a function of laser-pulse energy, single-shot exposure time, and scanning speed. Basic simulation, experimental setup, sample processing techniques, and cautionary remarks on stress and other related issues are discussed. In addition, we show that the nonlinear velocity dependence of TPA photopolymerization can be used as the shutter mechanism for disruptive 3D lithography. This mechanism, when combined with low numerical-aperture optics is exploited for the rapid microfabrication of ultrahigh-aspect-ratio (up to 50:1) photoplastic structures.

II. SU-8: COMPOSITION, CHEMICAL REACTIONS, AND PROPERTIES

SU-8 is an epoxy-based, near-UV, negative tone resist. The main component of the resist is EPON® SU-8 resin (Shell Chemical), which is dissolved in an organic solvent [gamma-butyrolacton (GBL)]. The amount of solvent determines the viscosity and thus, the range of available thicknesses, extending from tens of nanometers to millimeters. The resin is photosensitized as much as 10 wt % of the resin mass with triarylsulfonium salt, such as the CYRACURE® UVI (Union Carbide) with peaks of UV light absorption at 310 and 230 nm, allowing protolysis in the wavelength range of conventional broadband mask aligners.[19,26] Figure 1(a) shows the molecular structure of SU-8 (left: monomer; right: monomer unit in the crosslinked polymer) with eight epoxy sites per monomer. This demonstrates high epoxide functionality per molecule, which allows a high degree of crosslinking to be obtained to give high AR and straight sidewall profiles after exposure. In the crosslinking process, the epoxide monomers, stimulated by the curing agents, are transformed from a low-molecular weight melt to a highly crosslinked network.[26] The high epoxide functionality gives SU-8 its high chemical and thermal resistances (fully crosslinked glass-transition temperature, $T_g > 200\ ^\circ\mathrm{C}$ and degradation temperature, $T_d \sim 380\ ^\circ\mathrm{C}$) as well as good mechanical properties (Young's modulus, $E \sim 4-5$ GPa and biaxial modulus of elasticity, $E/(1-\nu) \sim 5.2$ GPa).[19,26] Polymerization of SU-8 is based on chemical amplification. A single photoevent, known as protolysis, initiates a cascade of subsequent chemical reactions that induce the crosslinking process. Figure 1(b) shows the generation of acid upon UV exposure as a result of protolysis of triarylsulfonium hexafluorantimonium, the cationic photoinitiator. Figures 1(c) and 1(d), respectively, show how this photoacid initiates the cationic ring-opening polymerization of the epoxy groups and how the chain propagation of the crosslinking process occurs. The photoacid is not consumed in the initiation pro-

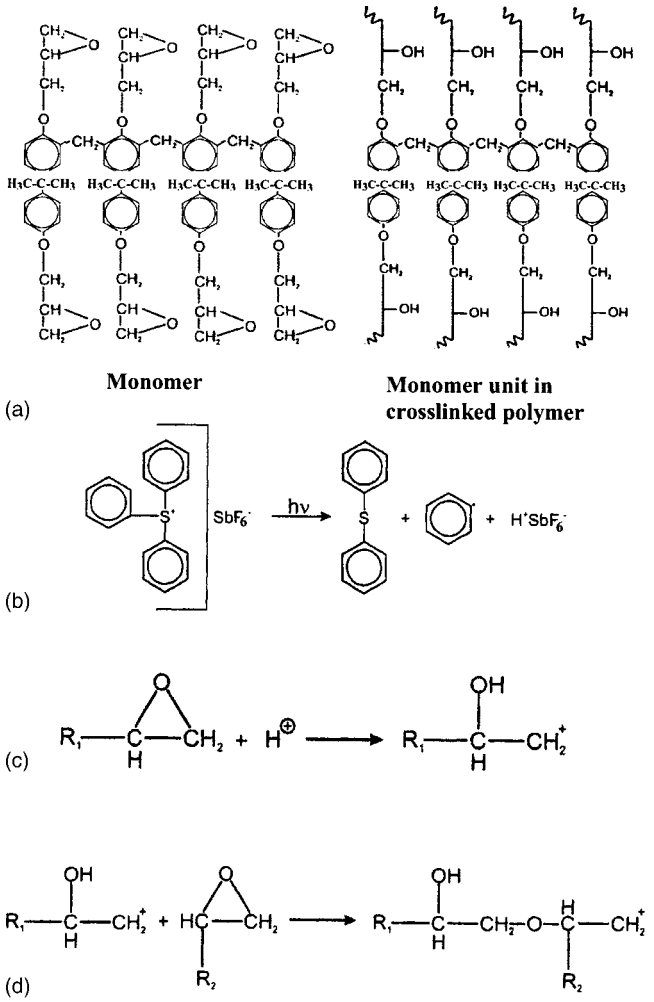

FIG. 1. (a) Molecular structure of EPON SU-8: The monomer (left) and the monomer unit in the crosslinked polymer (right). (b) Generation of acid upon UV exposure as a result of protolysis of triarylsulfonium hexafluorantimonium, the cationic photoinitiator. (c) Initiation of polymerization (crosslinking) via opening of the epoxy group. (d) Chain propagation of the crosslinking process. Figures are adapted from Ref. 26.

TABLE I. Physical properties of SU-8 photoresist, as adapted from Ref. 26.

Property	Value	Ref.
Young's modulus E (postbake at 95 °C)	4.02 GPa	19
Young's modulus E (hardbake at 200 °C)	4.95±0.42 GPa	26
Biaxial modulus of elasticity $E/(1-\nu)$	5.18±0.89 GPa	26
Film stress (postbake at 95 °C)	16–19 MPa	26
Maximum stress (hardbake at 200 °C)	34 MPa	26
Friction coefficient μ_F (postbake at 95 °C)	0.19	19
Glass temperature T_g (unexposed)	~50 °C	18
Glass temperature T_g (fully crosslinked)	>200 °C	18
Degradation temperature T_d (fully crosslinked)	~380 °C	18
Thermal expansion coefficient α (postbake at 95 °C)	52±5.1 ppm/K	26
Polymer shrinkage	7.5%	22

cess and can function to initiate several chains. The crosslinking process ultimately yields a dense, stable network where each epoxy monomer is connected to seven others on average.[26]

The invention and development of SU-8 at IBM Research[18–20] were triggered by the increased activity in micromachining and the need for high-AR, thick-film resist systems.[26] Some of its most attractive attributes include: low-cost and easy to obtain, low optical absorption in near-UV, good thermal and chemical stabilities (to be used as masks for prolonged reactive-ion etching), good resolution with vertical sidewall profiles (to be used as templates for electroplating in low-cost lithography, electroplating and molding applications), small Young's modulus (for the fabrication of highly compliant plastic micromechanical structures), and ultrathick spin-on coatings. A table of some of the most interesting mechanical and chemical properties of SU-8 photoresist is given in Table I.[26]

III. PRINCIPLES OF TWO-PHOTON ABSORPTION

SPA and TPA follow different selection rules. TPA consists of the excitation of a system from its initial state E_i to its final state E_f via a virtual intermediate state E_v. Under sufficient illumination intensity (typically achieved by high-peak-power laser), conventional electronic transitions caused by the absorption of a single photon of energy hf_1 may be produced by the simultaneous absorption of two photons of energy hf_2, each photon providing half the energy of the transition $(hf_1/2)$. TPA can occur in all media with or without inversion symmetry and is derived from a third-order susceptibility, which is distinct from second-harmonic generation (second-order susceptibility).[34] The transition probability of TPA was derived by Göppert-Mayer[35] using second-order perturbation theory.[36] Being a higher-order process, its absorption cross-section δ (~ of the order of 10^{-58} m^4 s/photon) (Ref. 9) is often many orders of magnitude smaller than that of SPA.[36] Because the absorption probability (AP) of TPA depends quadratically on the incident intensity I with TPA rate $R=\delta I^2$, this results in a narrower excitation in 3D space, and thus, real 3D objects can be fabricated by scanning the focal spot of the laser inside the photopolymer media. However, one should note that because of this nonlinearity, the voxel size depends more sensitively on laser intensity variation for TPA than SPA, thus requiring better intensity control to maintain repeatability.

IV. COMPARATIVE SIMULATION STUDY BETWEEN SPA AND TPA

In the experiments, the laser beam goes through the objective lens of the microscope and, thus, will be spatially filtered by its aperture, causing the light intensity distribution in the focal plane to arise from Fraunhoffer diffraction. For simplicity, a nominal Gaussian output of the laser going through a circular aperture is assumed to have a radial distribution of the radiant flux density in the focal plane to follow that of Airy,

$$I(x) = [2J(x)/x]^2 I_0, \tag{1}$$

where J_n represents the Bessel function and $x=2\pi na\xi/\lambda$, with n, a, ξ, and λ being the index refraction of the medium, aperture radius, angular function,[37] and wavelength, respectively. For a beam perpendicular to the focal plane, ξ reduces to $\sin\theta$.[37] Using small-angle approximation, $\sin\theta \approx \tan\theta = r/f$ with r being the radial distance and f the focal distance of the optics used. The distance between the aperture and the focal spot is assumed to be approximately f. Combining this with the optics (where $n=1$), we get $x=2\pi \mathrm{NA}r/\lambda$. Based on the simulation of Eq. (1) with $x=2\pi \mathrm{NA}r/\lambda$, Fig. 2 demonstrates the achievement of SDL resolution by TPA using 0.30-NA objective lens and $\lambda=796$ nm with the solid and dashed lines representing SPA and TPA, respectively. It should be noted that deviation from this simulation is possible due to oversimplification in the model. Nevertheless, it can be seen that by adjusting the laser intensity at the focal point to be above the TPA photopolymerization threshold [curves b and c in Fig. 2(a)], the diffraction limit simply becomes a measure of the focal spot size without putting any actual restraint to voxel sizes.[14] This is because TPA lithography involves direct laser writing, which deals with only one beam, whereas for SPA [curve d in Fig. 2(a)] in conventional lithography, the lateral size (w) of the solidification is limited by Rayleigh's criteria at 3.24 μm ($w=1.22\lambda/\mathrm{NA}$) due to signal overlapping from neighboring object points.[38] The quadratic dependence of the TPA rate on the incident intensity confines excitation to a focal volume (which is also optics NA and TPA photopolymerization threshold dependent), allowing real 3D microfabrication. The high-peak-power light, whose λ is too red for conventional SPA of SU-8, allows TPA due to the peak intensity in the focal volume. With adequate peak intensity, the AP becomes appreciable for the photoinitiator in SU-8 to absorb two long-λ photons simultaneously, combining their energy to reach its excited state. Figure 2(b) shows that the TPA distribution also suppressed oscillatory wings commonly found in SPA. Figures 2(c)–2(f) show 3D contour plots (AP cutoff at 0.5) for curves d, c, b, and a, respectively, with the insets of Figs. 2(c) and 2(d), illustrating the corresponding 2D contour plots for AP cutoff at 0.01.

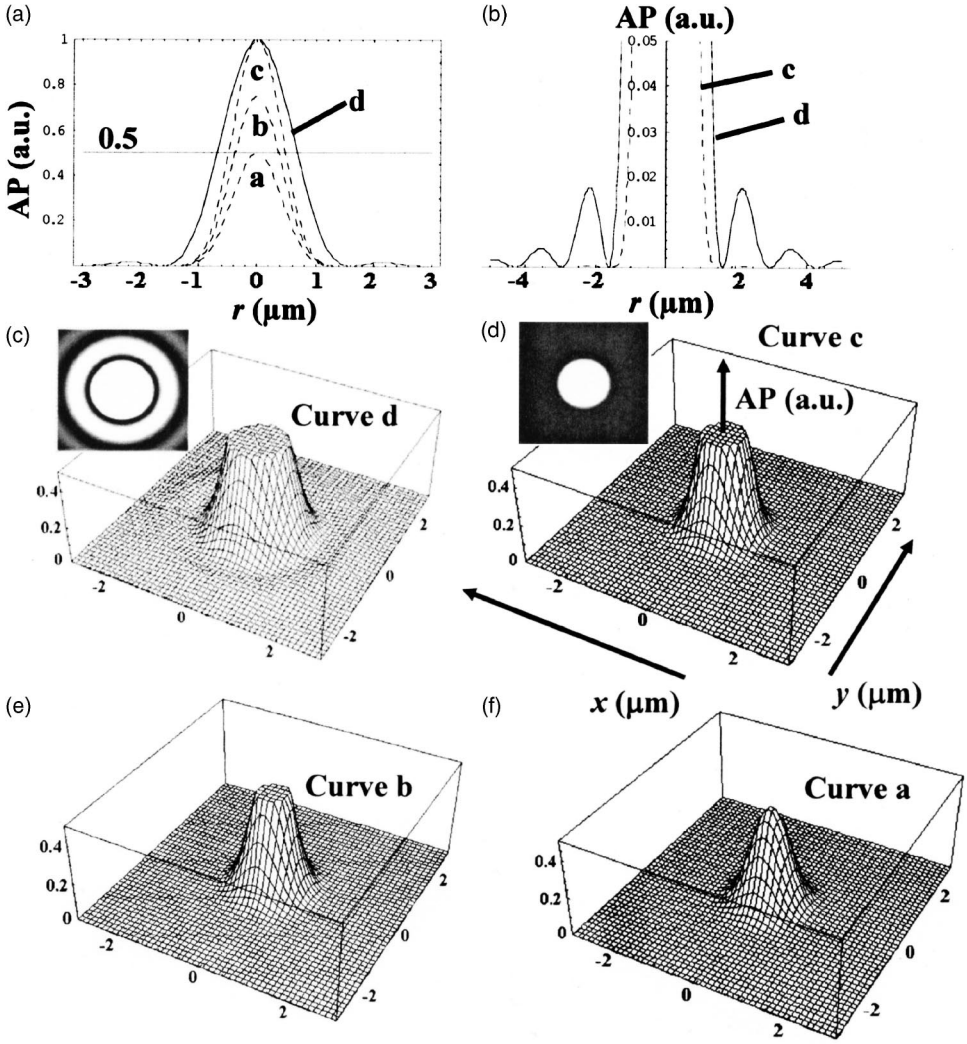

FIG. 2. Achievement of subdiffraction-limit resolution by TPA based on 0.30 NA and $\lambda = 796$ nm. (a) The absorption probability (AP) of SPA and TPA is given by solid and dashed curves, respectively. TPA curve a denotes the laser-pulse energy (LPE) to be right at the TPA-photopolymerization threshold while curves b and c above the threshold. Curve d represents SPA. (b) The existence of low amplitude oscillatory wings in SPA (curve d) is shown by having the AP cutoff at 0.05 and compared to TPA (curve c). (c)–(f) show 3D contour plots for curves d, c, b, and a, respectively. Insets of (c) and (d) illustrate 2D contour plots for AP cutoff at 0.01 for curves d and c, respectively.

V. EXPERIMENT

The samples used for this experimental work are SU-8 (Microresist technology GmbH) spin coated on buffered hydrofluoric (BHF)-rinsed (100) Si with prebaking (at 95 °C) time ranging from 15 min–10 h depending on the spin-on SU-8 thickness (which in this case, is between 975 nm and 500 μm thick). The time needed to prebake the SU-8 coatings increases exponentially with increasing thickness. BHF treatment is necessary to improve adhesion of SU-8 on Si by dissolving the native oxide on it. This step is crucial to avoid the fabricated structures from being washed away during the development step after TPA exposure. Occasionally, for dehydration and better removal of organic compounds, we subjected the samples to a bake at 200 °C for 15 min, followed by oxygen plasma ashing (Technics Plasma GmbH 100-E Plasma System) of 5 min at 300 W and 1-Torr O_2, both before the BHF rinse. After preparing the samples, TPA exposure follows by using the optical setup shown in Fig. 3. Independent of the thickness of the SU-8, all samples are postbaked at 95 °C for 15 min immediately after exposure. SU-8 crosslinking occurs during this step in regions that contain the acid catalysts generated during exposure. This bake is important because very little reaction takes place in the solid state where molecular motion is effectively frozen.[26] Nevertheless, the densification caused by the crosslinking process and outgassing of solvent results in only about 7.5% polymer shrinkage,[26] making it ideal for micromachining purposes. The TPA-processed samples were then developed carefully in propylene glycol methyl ether acetone (PGMEA), isopropanol (IPA) rinsed, and N_2 gas blown dry. Samples were sputtered with about 20 nm of Au (Balzers

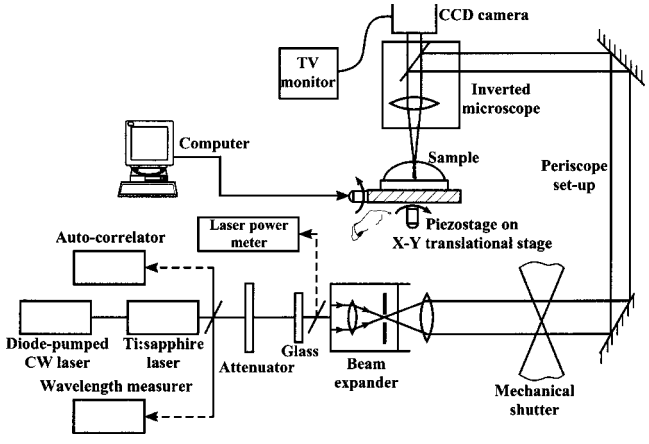

FIG. 3. Experimental setup for two-photon disruptive 3D lithography using femtosecond-pulsed near-IR Ti:sapphire laser.

SCD 030) before scanning electron microscopy (SEM) (Leo Gemini) inspection to minimize absorption during imaging.

As the lithography light source, we use an 80 MHz, 796-nm mode-locked Ti:sapphire laser (Tsunami, Spectra-Physics) with ~69-fs pulses and energies varying from 0.25 to 5.06 nJ/pulse (Ave. power: 20-405 mW). The pulse half-width of ~69 fs was determined by multiplying a 0.648 prefactor to the measured autocorrelation half-width based on a $\mathrm{sech}^2(x)$ real pulse shape. The power was measured by directing the beam into a power measurer (Fieldmaster LMI Coherent). The Ti:sapphire laser was excited by a diode-pumped, continuous-wave (cw) $Nd:YVO_4$ laser (Millennia Xs, Spectra-Physics) providing a green 532-nm output at 7.6 W. The laser beam goes through an adjustable optical intensity attenuator before being expanded and collimated by a beam expander setup. It then goes through an independent mechanical shutter with shutter speeds ranging from 4 ms to 2 s. Using a periscope, the laser pulses are coupled into an inverted microscope, to be reflected downwards by an infrared (IR) mirror (near 100% reflection for 700 nm $<\lambda<900$ nm by Laser Components GmbH), and then focused by a 0.30-NA, 10× objective lens into the sample, which is placed on a computer-controlled three-axis piezostage (Nanocube, Physics Instruments) affixed on a normal two-axis translation stage for flexibility. Laser-spot scanning on all three axes was provided by the relative movement of the piezostage, capable of rapid positioning operations of $100\times100\times100\ \mu m^3$ with nanometer-range resolution. The focal image on the sample is observed by a charge-coupled device (CCD) camera (Kappa CF11/2) coupled to a TV monitor (SONY HR Trinitron).

VI. RESULTS AND DISCUSSION

A. Characterization based on single-shot exposures

For this part of the experiment, a 975-nm-thick SU-8 coating on BHF-treated Si was obtained by spinning SU-8 2 at 6000 rpm for 30 s. We systematically exposed a 975-nm-thick SU-8 resist by focusing the laser at the SU-8/Si interface as a function of different laser-pulse energies (LPEs) and exposure time t. The choice of a thinner SU-8 layer is to ensure that solidification of SU-8 can easily occur at the SU-8/Si interface without requiring too tight control over the actual position of the focal spot of the laser. This is necessary to ensure adhesion to the Si substrate. The results of these experiments are shown in Figs. 4–6. Figures 4 and 5 show quantitative experimental evidence of SDL photopolymerization of voxels. In Fig. 4, the voxel diameter, as measured by the SEM, is plotted as a function of laser exposure time t for different laser average power (20–405 mW), whereas Fig. 5 shows the voxel diameter as a function of LPE for different laser exposure time t(4–1000 ms). Linear [see Figs. 4(a) and 5(a)] and logarithmic [see Figs. 4(b) and 5(b)] coordinates are used in both cases. From Figs. 4 and 5 it can be seen that an approximate logarithmic dependence of voxel size on exposure time and LPE (or collectively, the exposure dose) can be obtained. This is similar to those reported elsewhere[1,14] and can be explained by the exponential decay of the monomer concentration versus exposure. Because we use only one beam, the issue of Airy pattern light intensity overlapping is unfounded and thus, SDL photopolymerization can be achieved, provided that the photochemical processes responsible for the solidification, have a threshold response to light excitation.[1]

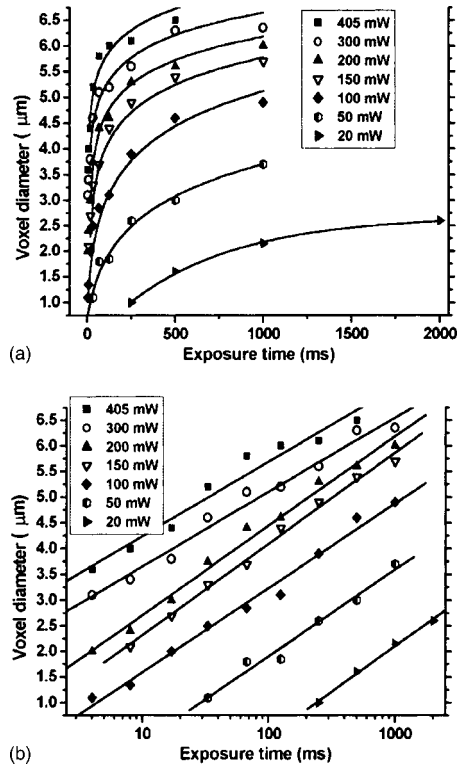

FIG. 4. Experimental evidence of subdiffraction-limit photopolymerization of voxels. Voxel diameter as a function of laser exposure time for different laser average power (20–405 mW) plotted with (a) linear and (b) logarithmic coordinates.

In this work, we found that off-the-shelf SU-8 with conventional photoacid generators (PAGs) has a good light intensity threshold for TPA at 796 nm. Although these PAGs are known to have a low TPA cross section, contrary to the experience of Kuebler *et al.*,[31] we can easily achieve a suitable high-resolution crosslinking with a big processing window without damaging the SU-8 material. The inset of Fig. 5(b) shows a SEM micrograph of a voxel exposed with a LPE of 1.25 nJ/pulse for 17 ms (circled data point). For the developed voxel, we notice a periodic modulation of its diameter along the beam propagation direction. This is caused by the back reflection from the SU-8/Si interface as a result of considerable refractive index mismatch ($n_{\text{SU-8}}\sim1.67$ to $n_{\text{Si}}\sim3.4$).[38]

Figure 6 tries to identify the laser-induced-damage (LID) dose in the SU-8 resist for (a) a fixed LPE of 5.06 nJ/pulse and (b) a fixed laser exposure time of 1000 ms. Similar to others,[8] it was found that a continuous increase of laser exposure time and/or LPE will result in the boiling of the SU-8, with a SEM micrograph example shown in the inset of Fig. 6(a). More specifically, LID occurs when the exposure time is more than 900 ms for a LPE of 5.06 nJ/pulse. By linearly fitting the experimental data in Fig. 4(b) using the least-square method and extrapolating the linear plots to zero voxel diameter, we obtain threshold exposure times of 173,

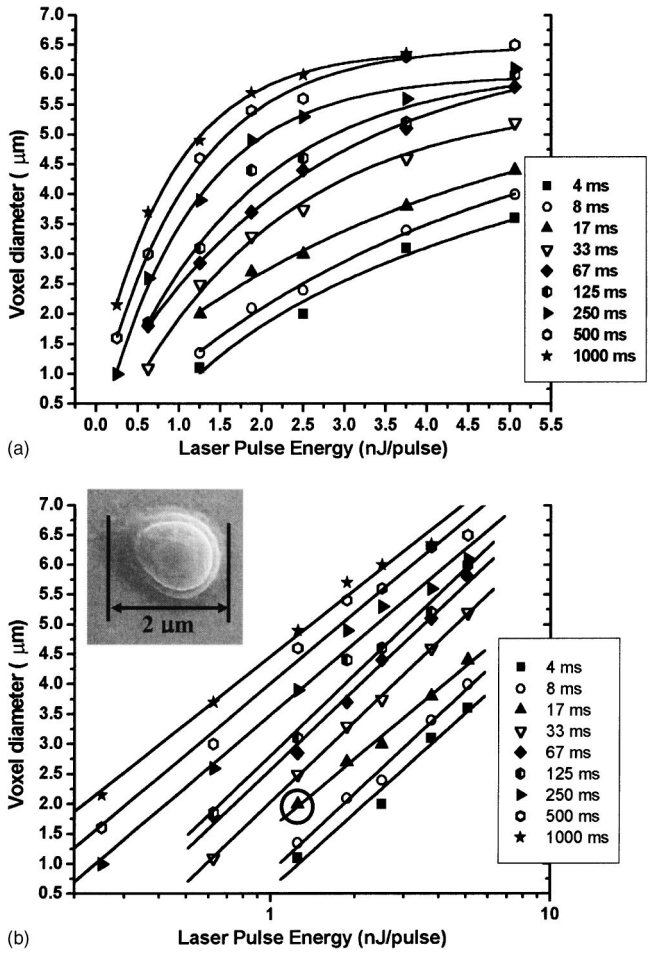

FIG. 5. Experimental evidence of subdiffraction-limit photopolymerization of voxels. Voxel diameter as a function of LPE for different laser exposure time (4–1000 ms) plotted with (a) linear and (b) logarithmic coordinates. Inset of (b) shows a SEM micrograph of a voxel exposed with a LPE of 1.25 nJ/pulse for 17 ms (circled data point).

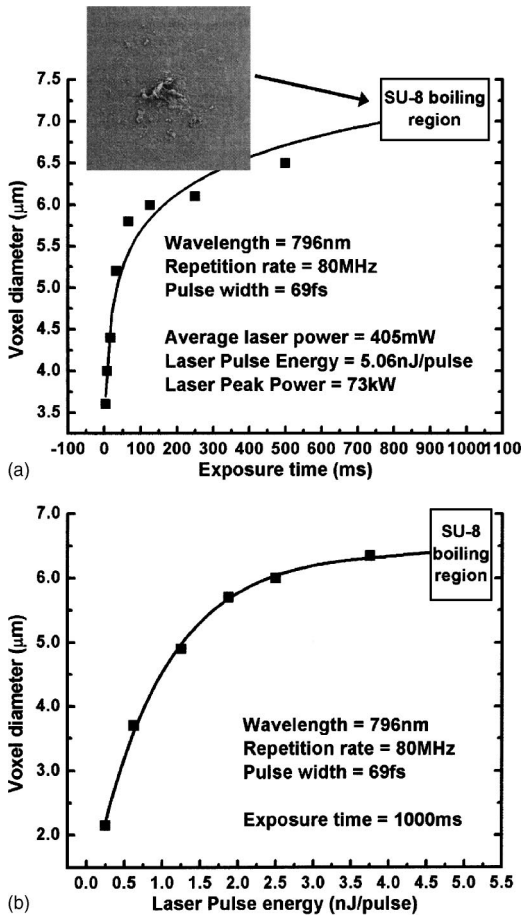

FIG. 6. Identifying the laser-induced-damage (LID) dose in the SU-8 resist for (a) fixed LPE of 5.06 nJ/pulse and (b) fixed laser exposure time of 1000 ms. Inset of (a): a SEM micrograph of a LID voxel.

21, 3.2, 1.3, 0.7, 0.1, and 0.04 ms for LPEs of 0.25, 0.63, 1.25, 1.88, 2.5, 3.75, and 5.06 nJ/pulse, respectively. We should caution that the voxel diameter that we have characterized is slightly overestimated due to additional secondary doses caused by backscattered photons. We did not include the longitudinal spatial resolution because of the limitations placed by the thickness of the SU-8 in this direction. Nevertheless, our earlier work[32] on using AFM to characterize the height of the voxels formed in a 5.4-μm-thick SU-8 resist (and hence not limited by its thickness) seems to suggest a spinning ellipsoid (or elongated sphere) voxel shape with a high AR due to the low-NA optics used consistent with those reported by others.[1,16,17] A systematic study[16] of the lateral and longitudinal dimensions of the voxels, including unexpected scaling laws,[17] has been reported by Sun *et al.* A common problem when using thick SU-8 resist for characterization purposes is the fact that the low-dimensional voxels get washed away during the development step due to poor adhesion, exacerbated by the high viscous force of the remaining uncrosslinked SU-8. Additional experiments also reveal that the absolute voxel size is extremely sensitive to the final laser dose that it receives (especially for lower exposure time and LPE), which may vary depending on the stability of the laser source and the attenuation sustained along its beam path. This high sensitivity to laser intensity, which may cause repeatability issues, is unfortunately a characteristic of TPA.

B. Characterization based on laser scanning speed

The dose and velocity dependence of TPA photopolymerization, important for the development of the "shutter" mechanism, are studied, with the results shown in Figs. 7 and 8. The samples prepared for this part of the experiment are similar to the experiments for the single-shot exposures. Here, we used a signal processor-based real time data-acquisition system (ADwin, Keithley) to systematically scan the laser focal spot in equally spaced straight lines with different scanning speeds v in the interior of the SU-8 resist based upon the relative movement of the piezostage (Nanocube, Physics Instruments). This is schematically shown in Fig. 7(a). To minimize backscattered effects, which may overestimate the actual linewidth, we focused the laser to be slightly above the SU-8/Si interface.

Figures 7(b)–7(e) show the experimental evidence (SEM micrographs) of SDL photopolymerization of SU-8 lines using LPEs of 1.25, 1.00, 0.75, and 0.50 nJ/pulse, respectively. For different lines of the same LPE, the scanning speeds (from left) are 2, 4, 8, 12, 16, 20, 25, 40, 50, 60, and

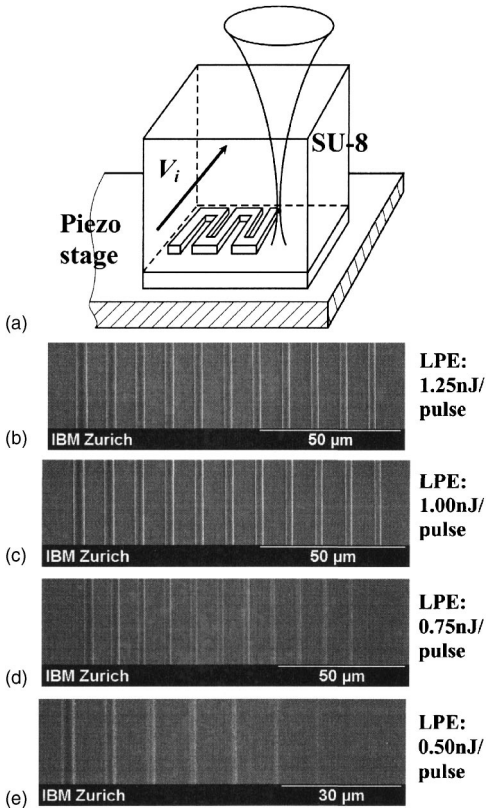

FIG. 7. Experimental evidence of subdiffraction-limit photopolymerization of SU-8 lines. (a) General schematic of how TPA-photopolymerized lines of different widths are exposed by exploiting different scanning speed v in a single sweep. (b)–(e) SEM micrographs of TPA-photopolymerized lines using LPEs of 1.25, 1.00, 0.75, and 0.50 nJ/pulse, respectively. For different lines of a common LPE, the scanning speeds (from left) are 2, 4, 8, 12, 16, 20, 25, 40, 50, 60, and 70 μm/s, respectively.

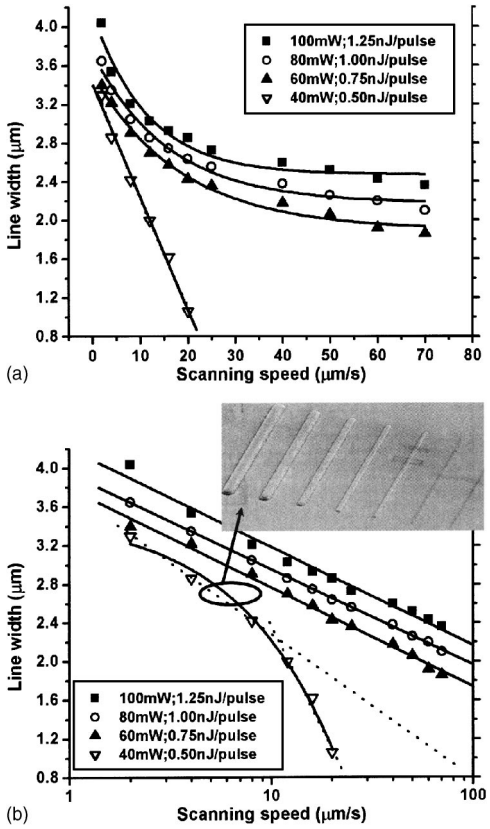

FIG. 8. Linewidth as a function of scanning speed for different LPEs in (a) linear and (b) logarithmic coordinates. Inset of (b): tilted SEM micrograph of a typical linewidth characterization experiment for a LPE of 0.50 nJ/pulse.

70 μm/s, respectively. Qualitatively, it was found that at significantly lower exposure doses (achieved with higher v and lower LPE), the edges of the lines become less abrupt with dendritic branches being observed. For example, at LPE $=0.50$ nJ/pulse, dendritic edges arise at $v=2$ μm/s while pores (with an average diameter of 10 nm) begin to appear at $v=20$ μm/s, indicating incomplete photopolymerization. Nevertheless, it is obvious from the results that the width of the photopolymerized SU-8 lines can be well controlled by scanning at different speeds with different LPEs. This dependency enables good control of the photopolymerized linewidths and facilitates the fabrication of disrupted 3D patterns in a rapid yet simple fashion without having to use a computer-controlled shutter. This is because by scanning at higher speeds (and depending on the LPE used), the exposure dose will simply not be high enough to exceed the TPA-photopolymerization threshold. The quantitative results are given in Fig. 8 in the form of linewidth as a function of scanning speed for different LPEs in (a) linear and (b) logarithmic coordinates. The inset of Fig. 8(b) shows a SEM micrograph (tilted) of a typical linewidth characterization experiment for LPE of 0.50 nJ/pulse. From Fig. 8, it is clear that the linewidth decreases as the scanning speed goes higher for a given LPE. An approximate logarithmic function of linewidth versus scanning speed can be found for LPE of 0.75, 1.00, and 1.25 nJ/pulse by linearly fitting the experimental data using the least-square method [see Fig. 8(b)]. These results are similar to those reported for other media[1,14] and can be explained by the inverse linear function of scanning speed versus exposure time. When the linear lines were extrapolated to zero linewidth, one can obtain threshold scanning speeds v_{th} of about 13 300, 9300, and 4800 μm/s for LPE of 1.25, 1.00, and 0.75 nJ/pulse, respectively. As for LPE$=0.50$ nJ/pulse, a first-order exponential decay curve was fitted to the data, which results in two distinct gradients intersecting at a v of 11 μm/s. Extrapolating the steeper gradient gives a v_{th} of 36 μm/s for LPE$=0.50$ nJ/pulse. The rapid drop in linewidth as a function of scanning speed may be explained by the incomplete protolysis of the cationic photoinitiator in SU-8 caused by insufficient activated states, as the dose goes below a certain threshold. This property is important to realize the shutter mechanism to fabricate disruptive 3D patterns.

C. Two-dimensional lithography based on TPA

By using the results shown in Figs. 7 and 8, a well-controlled 2D lithography of disruptive and nondisruptive structures is demonstrated by TPA, exposing an IBM logo using different scanning speeds and LPEs. The schematic shown at the top of Fig. 9 shows how these disruptive patterns are microfabricated in a well-controlled fashion using the velocity-dependent shutter mechanism. The IBM logo was patterned by TPA on a 975-nm-thick SU-8 layer with a v

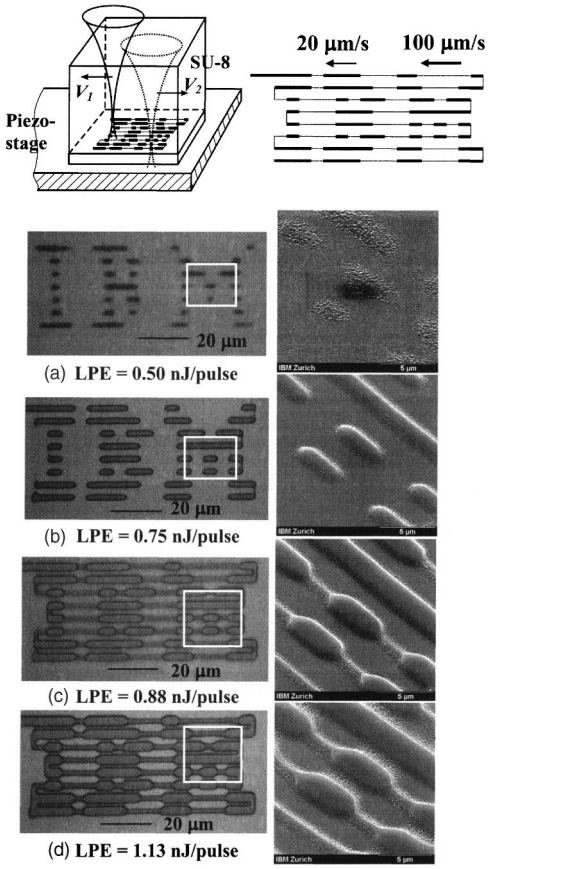

FIG. 9. Examples of well-controlled disruptive and nondisruptive 2D lithographies using the TPA technique: the IBM logo. Various LPEs (0.50–1.13 nJ/pulse) were used with scanning speeds of 20 and 100 μm/s. Corresponding micrographs (optical; left and SEM; right) are shown with the SEM micrographs on the right, showing a magnified view of the boxed area on the left. Top: general schematic for the microfabrication of the IBM logo using single-sweep two-photon lithography with variable scanning speeds. The main feature lines of the IBM logo were realized with a scanning speed of 20 μm/s (thick solid lines) while the discontinuity in between (thin solid lines) was scanned at 100 μm/s.

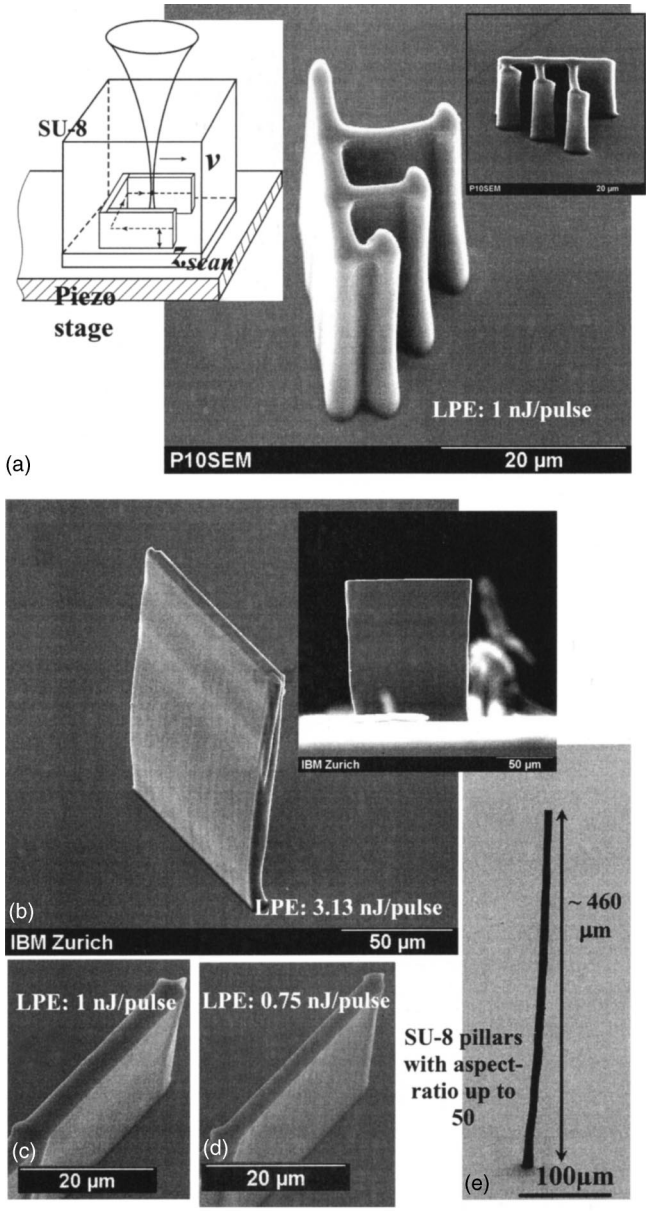

FIG. 10. Examples of rapid high-aspect-ratio (AR) microfabrication using the TPA technique based on low numerical-aperture optics. SEM micrographs of (a)–(d) vertical photoplastic planes (AR up to 23:1) and (e) photoplastic pillars (AR up to 50:1). The top left inset of (a) shows the general schematic of how vertical planes are fabricated using single-sweep TPA exposure based on different scanning speeds v and z_{scan} positioning.

of 20 μm/s for the main line features while a v of 100 μm/s is used for the "discontinuity" in between. LPEs of 0.50, 0.75, 0.88, and 1.13 nJ/pulse were used for comparison purposes. Figures 9(a)–9(d) show the results of the microfabrication in the form of optical (left) and SEM (right) micrographs. It can be seen that as the LPE of the lithography light source increases, the width of the IBM lines becomes larger. In other words, a lower LPE results in lower photopolymerized line thickness and width. Also, the previously disruptive lines in between the main lines of the IBM logo become more apparent as LPE increases. Fully disruptive features of the IBM logo are only realized when the two lowest LPEs are used, namely, 0.50 and 0.75 nJ/pulse. Using these LPEs, the scanning speed of 100 μm/s is fast enough to provide such a low dose that the SU-8 is not photopolymerized by TPA. This speed is, however, not fast enough for the higher LPEs of 0.88 and 1.13 nJ/pulse. The dendritic branching effects, as observed in the line characterization experiments earlier, can also be seen in Fig. 9.

Figure 10 shows how the velocity-dependent shutter mechanism, when combined with low-NA optics, will enable the fabrication of ultrahigh-AR vertical structures, such as planes and pillars. This is done in a rapid, single-sweep manner in thick SU-8 resist without having to trace out the entire volume of the structure. By using low-NA optics, an individual voxel has a reasonably high AR and thus, when the laser focal spot is scanned at a velocity v at a predetermined height z_{scan} above the Si substrate, high-AR volumes can be traced out rapidly. The inset of Fig. 10(a) shows the schematic for this rapid TPA process based on different v and z_{scan}. The results shown in Figs. 10(a), 10(c), and 10(d) are based on TPA exposure on a 23-μm-thick SU-8 on Si. The structures shown in Figs. 10(b) and 10(e) are, respectively, realized on a 132-μm-thick SU-8 (prebaked for 3 h at 95 °C) and a 500-μm-thick SU-8 (prebaked for 10 h at 95 °C) on Si. Figure 10(a) shows a TPA-fabricated branch-

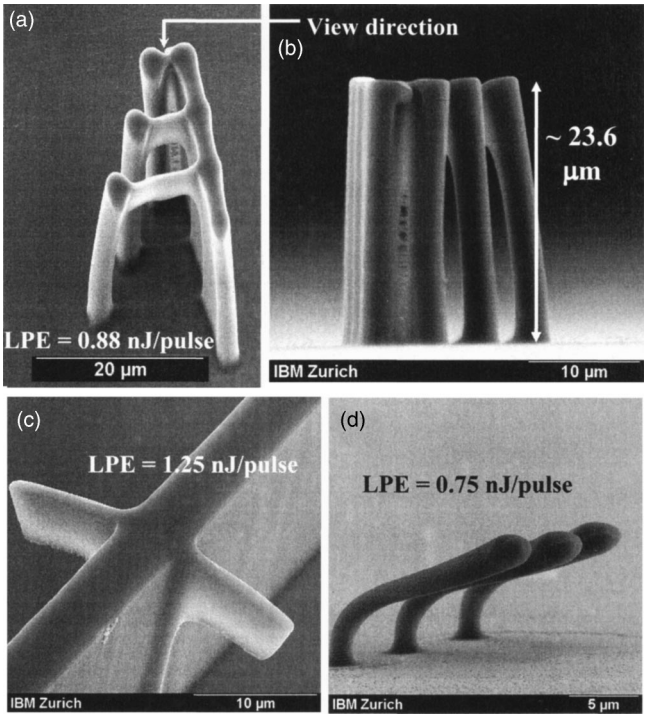

FIG. 11. Examples of real three-dimensional microfabrication using the TPA technique. SEM micrographs of (a) and (b) suspended photoplastic bridges of various lengths, (c) photoplastic microflaps, and (d) photoplastic cantilever rods.

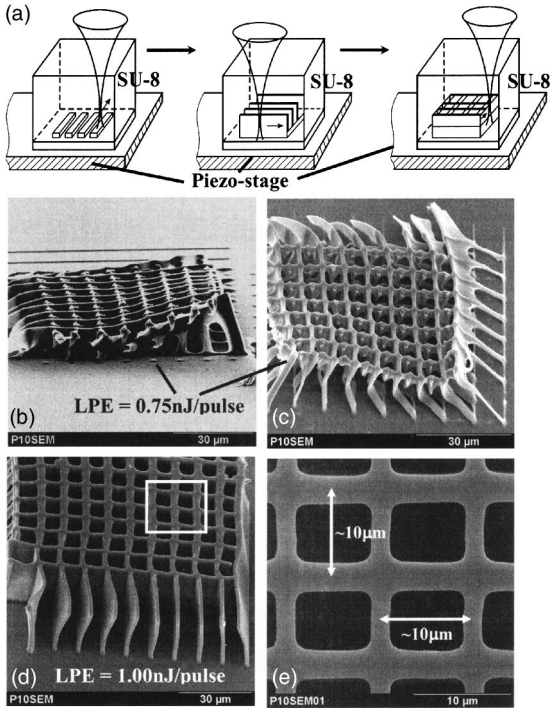

FIG. 12. Stress-control challenges associated with SU-8 TPA lithography. (a) General schematic showing how multilayer periodic structures are fabricated using TPA, (b)–(e) SEM micrographs of fabricated 3D periodic structures using different LPE, highlighting the importance of mechanical stability for multilayer SU-8 structures. (e) is a magnification of the boxed region in micrograph (d).

ing array of three vertical photoplastic planes extending to 5, 10, and 15 μm long with a height of 23 μm (which is limited by the resist). These vertical planes are produced by sweeping the laser focal spot (with a LPE of 1 nJ/pulse) at a v of 10 μm/s and a z_{scan} of 15 μm. To increase the mechanical stability of the planes, supporting pillars with bigger diameters were fabricated by scanning at 2 μm s^{-1} from $z_{\text{scan}}=0$ to 15 μm at both ends of the individual planes. An ultrahigh-AR line writing with a low NA of 0.30 is demonstrated in Figs. 10(b) and 10(e), where vertical photoplastic planes (122 μm high $\times$ 100 μm long $\times$ 5.3 μm width) with an AR of 23:1 as well as photoplastic pillars ($\sim$460 μm high $\times$ 8.2 μm diameter) with an AR of 50:1 are shown. The former is fabricated by tracing the focal spot of the laser horizontally (at LPE=3.13 nJ/pulse, $z_{\text{scan}}=40$ μm, $v=2$ μm s^{-1}, and in a single sweep of 50 s) while the latter, vertically (at LPE=3.75 nJ/pulse from $z=0-460$ μm at about 1–3 μm s^{-1}) through the interior of the thick SU-8 resist. To fabricate the extremely high vertical pillars, the focal spot of the laser has to be traced by hand due to the spatial limits of the piezostage. The pillars (seen at 45° tilt) were mechanically stable with no pedestals found around them, verifying the sharp rise of the TPA threshold. The stability is a result of the good mechanical properties of crosslinked SU-8 and also the large area (52.8 μm^2) for adhesion at its base. Meanwhile, Figs. 10(c) and 10(d) compare the different width of planes formed from the different LPEs (1.00 and 0.75 nJ/pulse) used, both scanned at a v of 2 μm/s. As anticipated, the width of the planes increases as LPE increases.

D. Real three-dimensional lithography based on TPA

Figures 11–13 demonstrate the inherent utility of TPA in realizing real 3D lithography based on SU-8 as the matrix material. The nonlinear velocity dependence of TPA photopolymerization is used as the shutter mechanism for the disruptive features. Samples used for the results shown in Fig. 11 are 23-μm-thick SU-8 spun on Si. In Figs. 11(a) and 11(b), fabricated bridges of various lengths (5–15 μm long) suspended at about 21 μm above the Si substrate are shown. These bridges, fabricated using a LPE of 0.88 nJ/pulse are supported by photoplastic pillars of about 23.6 μm high (limited by resist) scanned at 2 μm s^{-1} from a z_{scan} of 0–15 μm. Due to the high intrinsic stress of crosslinked SU-8, it can be seen from Fig. 11(b) that at least two of the fabricated pillars, which support the 10- and 15-μm-long bridges are deformed. Using the SEM, the tip deflection of the furthest pillar in Fig. 11(b) is measured to be about 2.7 μm (to the left). This yields a radius of curvature R of 103.1 μm using the model relation $R=L^2/2\Delta$, where L is the height of the pillar and Δ is the tip deflection. For a singly clamped rod with an area moment of inertia I and an exerted point load F at the tip F is found to be about 7.5 μN based on standard beam equation, where $\Delta=FL^3/3EI$. To calculate I (which is found to be about 3.02×10^{-24} m^4), the model relation $I=\pi r_p^4/4$ for a solid cylindrical lever, where r_p is the radius (which is measured to be about 1.4 μm) is used. A Young's modulus value of $E=4.02$ GPa was assumed for the crosslinked SU-8. The spring constant k of the pillar structure is about 2.8 N/m based on the formula, $k=3\pi Er^4/4L^3$,

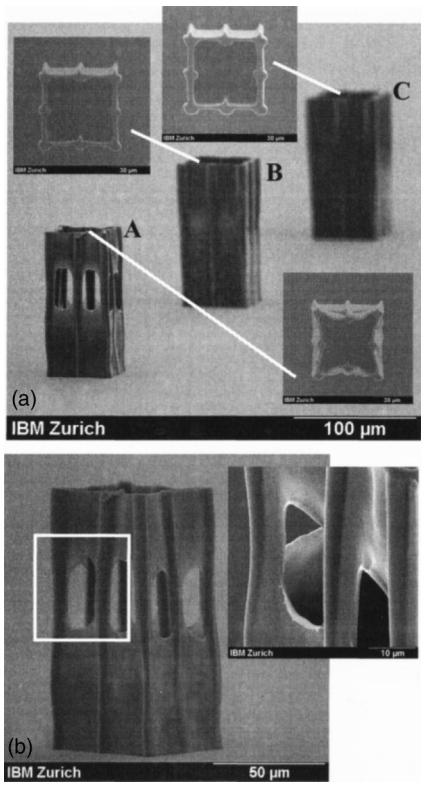

FIG. 13. SEM micrographs of (a) a $132\times50\times50$-μm^3 cage made from high-AR pillars and planes using a LPE of 0.75 nJ/pulse (cage A), 1.00 nJ/pulse (cage B), and 1.25 nJ/pulse (cage C) with insets showing the respective plan views and (b) cage A with the inset showing the magnification of the corresponding boxed area.

a value low enough for applications as high compliance photoplastic AFM probes.[26] The force F is caused by the stress in the bridges, which starts to relax upon development and is found to be higher for longer bridges. The remaining pillar (which supports the 5-μm-long bridge) remains straight due to some partial support given by the dendritic branches. These branches are the results of the superposition of adjacent doses caused by their close proximity. Figure 11(c) shows suspended flap structures fabricated with a LPE of 1.25 nJ/pulse with a v of 20 μm/s. As for the cantilever rods shown in Fig. 11(d), these were actually fabricated vertical pillars, which collapsed due to inadequate crosslinking (caused by a shorter postbaking time). This explains its near-circular cross sections.

Figure 12 illustrates application examples of using TPA lithography on SU-8 to micromachine 3D periodic structures for potential use in microphotonics. Figure 12(a) shows a general schematic on how multilayer periodic structures are fabricated, while Figs. 12(b) and 12(c) highlight the importance of mechanical stability for multilayer SU-8 structures as well as its associated stress-control challenges. The fabricated structures shown in Figs. 12(b) and 12(c) failed to provide adequate mechanical strength to support itself due to the narrow linewidth ($\sim$1 μm) caused by the lower LPE (0.75 nJ/pulse) exposure on the 23-μm-thick SU-8 on Si sample. By using a higher LPE of 1.00 nJ/pulse, thicker base supporting lines of about 2–3 μm in width were realized, providing mechanically stable and rigid structures with a measured periodicity of about 10 μm [see Figs. 12(d) and 12(e)]. Besides being more stable at the base, the successful fabrication of these upright periodic structures is due to the increased adhesion at the base (due to the larger contact area) as well as the fact that the sample is left to stress relax for about 15–20 min after postbaking before development. However, with the higher LPE, the real 3D profile is lost (resulting in an "egg-box" structure), as observed in Fig. 12(d) due to the merging of the layers above each other. The repeated lines in Fig. 12 were scanned at 10 μm/s with a periodicity of 10 μm based on the written program for the piezostage.

In Fig. 13, all three degrees of freedom provided by the piezostage were used to fabricate a cage structure, which is made from high-AR pillars and planes. Figure 13(a) shows SEM micrographs of the $132\times50\times50$-μm^3 cage made from high-AR pillars and planes using a LPE of 0.75 nJ/pulse (cage A), 1.00 nJ/pulse (cage B), and 1.25 nJ/pulse (cage C) with insets showing the respective plan views. The cages were patterned on a 132-μm-thick SU-8 on Si as two 50×50-μm^2 traces separated with a vertical displacement z_{scan} of 50 μm with the first (bottom) square trace focused at about 20 μm above the substrate. Due to the low-NA optics used, a single sweep of one of the square traces at 5 μm/s produces vertical planes measuring 50 μm high and 1.47 μm wide, resulting in an AR of 34. The ability to fabricate high-AR planes in a single sweep using low-NA optics avoids the need to trace out the entire volume of the plane. The entire cage structure ($132\times50\times50$ μm^3) was made in only 307 s. Similar to the periodic structures shown in Fig. 12, only cage A has a low enough LPE to preserve the real 3D profile while the other cages simply merge at the "window openings." For these structures, a similar relaxation time (typically 15–20 min) is provided after postbaking. Also, pillars were made (scanned at 2 μm/s giving a diameter of about 6.7 μm) to mechanically support the cage structure. However, as shown in the inset of Fig. 13(a), stress effects remain for the top square layer of cage A. Figure 13(b) shows cage A with the inset magnifying the corresponding boxed area. Due to the high AR of an individual voxel, it can be seen from the inset of Fig. 13(b) that the high-AR planes have minor peeling effects at the edges of the "windows." To circumvent this problem, higher NA optics will be used for future experiments, both to provide a more "spherical" voxel and also to get an easily achievable higher resolution.

VII. CONCLUSIONS

In summary, this work has presented, by far in the literature, one of the most comprehensive experimental studies of TPA in standard SU-8 resist, to be used for real 3D lithography. It has been conclusively shown that off-the-shelf SU-8 is indeed a good candidate matrix material for TPA photopolymerization. By combining the use of low-NA optics and the velocity dependence of TPA photopolymerization as the shutter mechanism, a well-controlled disruptive 3D lithography of high-AR photoplastic structures is successfully demonstrated.

This capability and set of characterization results will benefit the MEMS and optics community, enabling them to produce a quick prototyping of static and dynamic 3D structures. Experimentally, verified modulation of linewidths and voxel sizes with controlled laser-pulse energy, exposure time, and scanning speed yield resolution beyond the conventional SPA diffraction limit. More importantly, the quadratic dependence of absorption probability on light intensity in TPA allows real 3D lithography to be performed by confining the TPA-exposed area to a localized volume in the interior of the resist. Coupled with low-NA optics and a controllable piezostage, this work demonstrates the rapid processing of high-AR 3D structures without the use of a computer-controlled shutter. However, stress issues in SU-8 have to be solved before one can proceed to fabricate more complicated multilayer structures.

ACKNOWLEDGMENTS

The authors thank G. Salis, R. Harbers, R. F. Mahrt, M. Despont, and B. Gotsmann from IBM Zürich Research Laboratory for helpful technical discussions and support with the use of the optical setup, in particular, the Ti: sapphire laser. One of the authors (W.H.T.) thanks G. Salis for the simulations performed, IME for his scholarship, and IBM Zürich for the visiting scientist appointment.

[1]T. Tanaka, H.-B. Sun, and S. Kawata, Appl. Phys. Lett. **80**, 312 (2002).
[2]S. Maruo and K. Ikuta, Appl. Phys. Lett. **76**, 2656 (2000).
[3]A. Bertsch, H. Lorenz, and P. Renaud, Proceedings of the IEEE International Workshop on Micro Electro Mechanical Systems (MEMS '98), Heidelberg, Germany, 1998, pp. 18–23.
[4]T. Yu, C. K. Ober, S. M. Kuebler, W. Zhou, S. R. Marder, and J. W. Perry, Adv. Mater. (Weinheim, Ger.) **15**, 517 (2003).
[5]D. A. Parthenopoulos and P. M. Rentzepis, Science **245**, 843 (1989).
[6]B. H. Cumpston *et al.*, Nature (London) **398**, 51 (1999).
[7]W. Denk, J. H. Strickler, and W. W. Webb, Science **248**, 73 (1990).
[8]H.-B. Sun, S. Matsuo, and H. Misawa, Appl. Phys. Lett. **74**, 786 (1999).
[9]E. S. Wu, J. H. Strickler, W. R. Harrell, and W. W. Webb, Proc. SPIE **1674**, 776 (1992).
[10]S. Maruo, O. Nakamura, and S. Kawata, Opt. Lett. **22**, 132 (1997).
[11]S. Maruo and S. Kawata, J. Microelectromech. Syst. **7**, 411 (1998).
[12]G. Witzgall, R. Vrijen, E. Yablonovitch, V. Doan, and B. J. Schwartz, Opt. Lett. **23**, 1745 (1998).
[13]H.-B. Sun, T. Kawakami, Y. Xu, J.-Y. Ye, S. Matuso, H. Misawa, M. Miwa, and R. Kaneko, Opt. Lett. **25**, 1110 (2000).
[14]S. Kawata, H.-B. Sun, T. Tanaka, and K. Takada, Nature (London) **412**, 697 (2001).
[15]S. Maruo, K. Ikuta, H. Korogi, Proceedings of the IEEE International Microelectromechanical Systems Conference (MEMS '01), Interlaken, Switzerland, 2001, pp. 594–597; Proceedings of the IEEE-NANO, Maui, USA, 2001, pp. 507–512.
[16]H.-B. Sun, T. Tanaka, and S. Kawata, Appl. Phys. Lett. **80**, 3673 (2002).
[17]H.-B. Sun, K. Tanaka, M.-S. Kim, K.-S. Lee, and S. Kawata, Appl. Phys. Lett. **83**, 1104 (2003).
[18]N. LaBianca and J. D. Gelorme, Proc. SPIE **2438**, 846 (1995).
[19]H. Lorenz, M. Despont, N. Fahrni, N. LaBianca, P. Renaud, and P. Vettiger, Proceedings of the Micromechanics Europe Workshop (MME '96), Barcelona, Spain, 1996, pp. 32–35; J. Micromech. Microeng. **7**, 121 (1997).
[20]M. Despont, H. Lorenz, N. Fahrni, J. Brugger, P. Renaud, and P. Vettiger, Proceedings of the IEEE International Workshop on Microelectromechanical Systems (MEMS '97), Nagoya, Japan, 1997, pp. 518–522.
[21]H. Lorentz, M. Despont, N. Fahrni, J. Brugger, P. Vettiger, and P. Renaud, Sens. Actuators, A **64**, 33 (1998).
[22]L. J. Guerin, M. Bossel, M. Demierre, S. Calmes, and P. Renaud, Proceedings of the Transducers '97, Chicago, USA, 1997, pp. 1419–1422.
[23]C.-H. Lin, G.-B. Lee, B.-W. Chang, and G.-L. Chang, J. Micromech. Microeng. **12**, 590 (2002).
[24]G. Genolet, J. Brugger, M. Despont, U. Drechsler, P. Vettiger, N. F. de Rooij, and D. Anselmetti, Rev. Sci. Instrum. **70**, 2398 (1999).
[25]G. Genolet, M. Despont, P. Vettiger, D. Anselmetti, and N. F. de Rooij, J. Vac. Sci. Technol. B **18**, 617 (2000).
[26]G. Genolet, Ph.D. thesis, EPFL, Lausanne, Switzerland, 2001.
[27]I. Roch, Ph. Bidaud, D. Collard, and L. Buchaillot, J. Micromech. Microeng. **13**, 330 (2003).
[28]V. Seidemann, S. Bütefisch, and S. Büttgenbach, Proceedings of the Transducers '01, Munich, Germany, 2001, pp. 1616–1619.
[29]A. Bertsch, H. Lorenz, and P. Renaud, Sens. Actuators, A **73**, 14 (1999).
[30]X. Yin, N. Fang, X. Zhang, I. B. Martini, and B. J. Schwartz, Appl. Phys. Lett. **81**, 3663 (2002).
[31]S. M. Kuebler, K. L. Braun, W. Zhou, J. K. Cammack, T. Tu, C. K. Ober, S. R. Marder, and J. W. Perry, J. Photochem. Photobiol., A **158**, 163 (2003).
[32]W. H. Teh *et al.*, Proceedings of the 17th European Conference on Solid-State Transducers (Eurosensors XVII), Guimaraes, Portugal, 2003, pp. 783–786.
[33]W. H. Teh, U. Dürig, G. Salis, R. Harbers, U. Drechsler, R. F. Mahrt, C. G. Smith and H.-J. Güntherodt, Appl. Phys. Lett. **84**, 4095 (2004).
[34]E. Yablonovitch and R. B. Vrijen, Opt. Eng. **38**, 334 (1999).
[35]M. Göppert-Mayer, Ann. Phys. **9**, 273 (1931).
[36]Y. R. Shen, *The Principles of Nonlinear Optics* (Wiley, Toronto, 1984).
[37]J. D. Jackson, *Classical Electrodynamics* (Wiley, New York, 1975).
[38]T. Kondo, K. Yamasaki, S. Juodkazis, S. Matsuo, V. Mizeikis, and H. Misawa, Thin Solid Films **453–454**, 550 (2004).